Nanoscale

REVIEW

View Article Online
View Journal | View Issue

Cite this: *Nanoscale*, 2022, **14**, 11892

Advancing integrated CO_2 electrochemical conversion with amine-based CO_2 capture: a review

Mengran Li, *[a] Kailun Yang,[a] Maryam Abdinejad, [a] Chuan Zhao [b] and Thomas Burdyny *[a]

Carbon dioxide (CO_2) electrolysis is a promising route to utilise captured CO_2 as a building block to produce valuable feedstocks and fuels such as carbon monoxide and ethylene. Very recently, CO_2 electrolysis has been proposed as an alternative process to replace the amine recovery unit of the commercially available amine-based CO_2 capture process. This process would replace the most energy-intensive unit operation in amine scrubbing while providing a route for CO_2 conversion. The key enabler for such process integration is to develop an efficient integrated electrolyser that can convert CO_2 and recover the amine simultaneously. Herein, this review provides an overview of the fundamentals and recent progress in advancing integrated CO_2 conversion in amine-based capture media. This review first discusses the mechanisms for both CO_2 absorption in the capture medium and electrochemical conversion of the absorbed CO_2. We then summarise recent advances in improving the efficiency of integrated electrolysis *via* innovating electrodes, tailoring the local reaction environment, optimising operation conditions (*e.g.*, temperatures and pressures), and modifying cell configurations. This review is concluded with future research directions for understanding and developing integrated CO_2 electrolysers.

Received 16th June 2022,
Accepted 2nd August 2022

DOI: 10.1039/d2nr03310k

rsc.li/nanoscale

Introduction

Carbon dioxide (CO_2) electrolysis powered by renewable or low-carbon electricity is one of the promising routes to convert CO_2 into valuable chemicals, such as carbon monoxide (CO), formic acid, ethylene, and ethanol.[1–4] Recent years have seen a

[a]*Materials for Energy Conversion and Storage (MECS), Department of Chemical Engineering, the Delft University of Technology, van der Maasweg 9, 2629 HZ Delft, The Netherlands. E-mail: m.li-8@tudelft.nl, t.e.burdyny@tudelft.nl*
[b]*School of Chemistry, The University of New South Wales, Sydney, 2052 New South Wales, Australia*

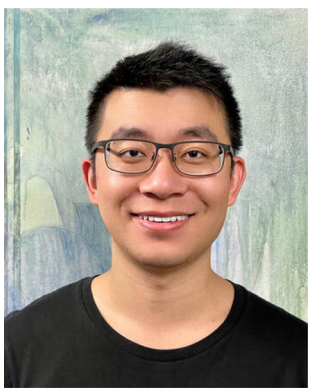

Mengran Li

Dr Li obtained his PhD degree at the University of Queensland (UQ), Australia in 2016, and then started his postdoc position at UQ on the development of viable CO_2 electrolysis technology for steel mills. His research in the field of CO_2 electrochemical reduction includes material and system development and experiment testing, with a goal of understanding electrode interfacial interactions and developing industrially relevant electrochemical processes via *material innovation and engineering. He will soon join the University of Melbourne as a Lecturer to continue his research and passion for material engineering and process innovation.*

Kailun Yang

Dr Yang completed her PhD degree at TU Delft in 2022. After graduation, she continued her research as a postdoctoral fellow in the same group advancing electrochemical CO_2 reduction to value-added products. Her main research interests lie in integrating renewable electricity into the energy transition process. Her research is mainly focused on improving the efficiency of electrochemical CO_2 reduction by optimizing multiphase transport in different CO_2 electrolyzer configurations. She is also interested in building and analyzing Multiphysics models to understand and predict the transport phenomena, and their relationship with the relevant reaction environment and performance.

remarkable advancement of this process in achieving industrially relevant current densities (up to over 1 A cm^{-1}) and high product faradaic efficiency by applying gas-diffusion electrodes.[5–7] However, the state-of-the-art CO_2 electrolysis usually uses pure CO_2 as the feed, while CO_2 is diluted in most industrial sources (<20% for flue gases from blast furnaces and post-combustion power plants[8–10]).[5,11–21] When implemented in practice, CO_2 electrolysis requires costly upstream CO_2 capture processes[22,23] to concentrate CO_2, and an energy-intensive product separation process[24,25] to recycle CO_2 and concentrate product streams. In addition, gaseous CO_2 reacts with hydroxide ions generated within CO_2 electroreduction systems to form (bi)carbonate.[6,26–29] The additional recovery of CO_2 from the (bi)carbonate is another energy-intensive process that usually demands >230 kJ $mol^{-1}_{CO_2}$.[30] In a zero-gap membrane electrode assembly configuration, the (bi)carbonates are also prone to precipitate at electrode pores, block CO_2 diffusion to the catalytically active surface, and severely degrade the overall cell performance.[7,31,32] These technical issues constitute the significant challenges faced by the practical deployment of gas-fed CO_2 electrochemical conversion at a large scale.

An emerging strategy to address these challenges is to intensify the CO_2 capture and electrochemical conversion processes.[33–35] A schematic illustration is shown in Fig. 1a and b. The CO_2 electrolysis process can potentially replace the energy-intensive stripper in the capture step. Sullivan *et al.*[33] recently defined such a coupled process as Type-III fully integrated processes, including direct electroreduction of CO_2 in amine-based, (bi)carbonate, and ionic liquids. As shown in Fig. 1c, the integrated electrolyser consists of an anode for water oxidation, an ion-conductive membrane, and a cathode that should be able to convert CO_2 to products and recover the capture medium simultaneously.[36,37] In the integrated conversion step, taking amine-based capture media as an example, the absorbed CO_2 in the liquid capture media becomes the primary CO_2 source for the CO_2 conversion instead of the gaseous CO_2. In this case, the coupled processes have the potential to prevent unwanted carbonation issues and achieve a concentrated product stream without significant downstream product separation if the conversion product is a gas product such as CO. In addition, such an intensification also has a promise of lowering the overall cost of the CO_2 capture by displacement of the regeneration unit and CO_2 compression.

Our recent energy analyses[36] over sequential and coupled routes revealed that about 42% of overall energy could be saved for the integrated route if the integrated electrolyser can be operated at the same energy efficiency (~1000 kJ $mol_{CO_2\ converted}^{-1}$) as the state-of-the-art gas-fed electrolyser (3 V and 90% CO faradaic efficiency). The development of the integrated electrolyser is the crucial step enabling a more efficient coupled process and further cost reduction for the CO_2 capture and utilisation. As amine scrubbing is the most commercially available CO_2 capture process for industrial exhaust, the scope of this review will focus on the development of integrated CO_2 electrolysis with amine-based CO_2 capture.

The development of the integrated CO_2 conversion is still at the early stage. Most studies still apply similar techniques and strategies implemented in gas-fed electroreduction to advance integrated CO_2 electroreduction. Most of the reported activity and product selectivity for CO_2 electroreduction in the amine-based capture medium is also inferior to the performance of gas-fed CO_2 conversion. As a result, the overall energy efficiency of the integrated electrolyser is much lower than the gas-fed electrolyser[36] and makes the overall process intensification less economically attractive than the sequential route.

This review aims to provide an overview of the most recent advances in improving CO_2 electroreduction, mainly in amine-based capture media, focusing on the unique features of CO_2 electroreduction in the capture media compared to the gas-fed

Maryam Abdinejad

Dr Abdinejad received her first and second MSc degrees in Pharmaceutical Science at the University of Greenwich/England and Molecular Science at Ryerson University/Canada, respectively. She obtained her Ph.D. from the University of Toronto/Canada and joined Professor Tom Burdyny's research group at the Delft University of Technology (TU Delft)/Netherlands in 2021 as a postdoctoral researcher. Her current research focus is on the rational design and development of novel high-performance homogeneous and heterogeneous catalysts for the electrochemical reduction of CO_2 to value-added materials.

Chuan Zhao

Professor Chuan Zhao is a full Professor at the School of Chemistry at the University of New South Wales (UNSW), Sydney. He also holds a Professorial Future Fellowship from Australian Research Council. He is interested in discovering novel electrochemical methodologies and nanomaterials for energy applications including water splitting, hydrogen fuel cells, CO_2 & N_2 reduction, batteries, and sensors.

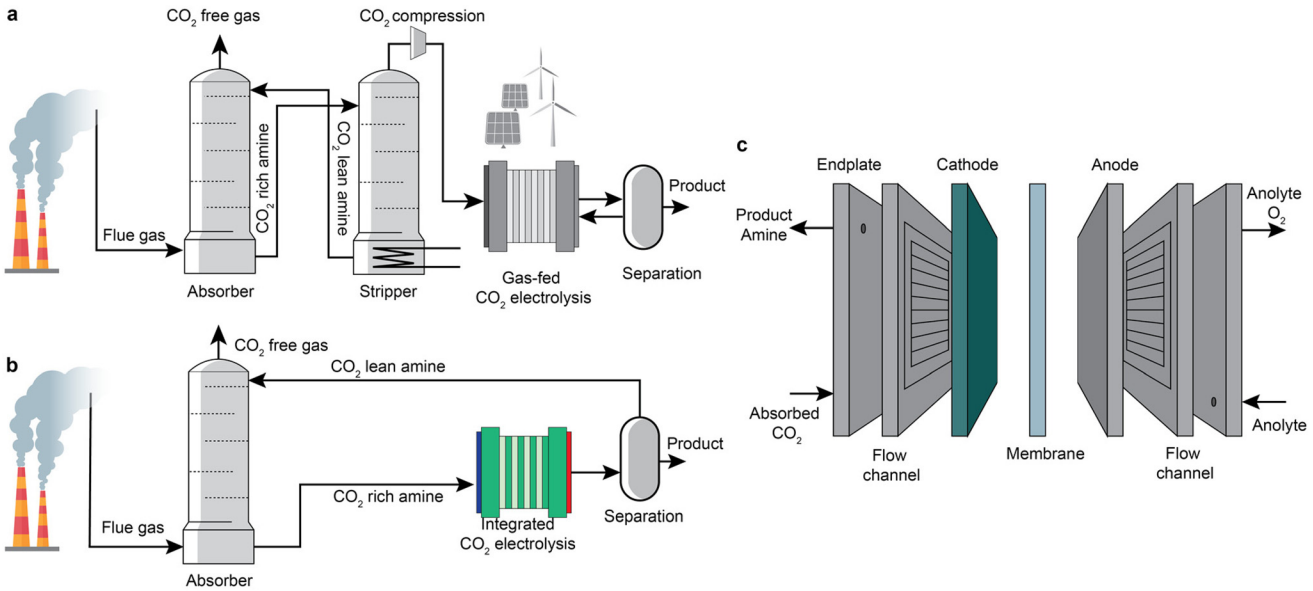

Fig. 1 Schematic illustration of (a) sequential CO_2 capture and electrolysis based on gas-fed electrolysers, (b) an integrated route based on integrated electrolysers, and (c) cell configuration of a single cell of the integrated electrolysers.

electroreduction. This review starts with the discussion of catalytically active species for CO_2 absorption in amines and potential catalytically active species available for CO_2 reductions in the capture media. In the following section, we summarise current strategies to advance integrated electrolysers *via* the development of electrodes, capture media, operating conditions (*e.g.*, temperature and pressure), and cell configuration. The review concludes with challenges and an outlook for developing efficient integrated CO_2 electrolysers. Through this review, we anticipate providing new insights that can benefit the understanding and development of the integrated CO_2 electrolysers.

Thomas Burdyny

Professor Burdyny completed his PhD from the University of Toronto (2017) followed by a brief postdoc at the Delft University of Technology. In 2019 he began his independent career at TU Delft, where his group focuses on applied and process integration aspects of electrochemical technologies, namely CO_2 reduction. Tom has been the recipient of the prestigious VENI personal grant (2019) from the Dutch government to pursue scale-up research of electrochemical technologies, as well as acting as the ethylene work package leader in the Horizon 2020 EU project SELECTCO₂. His work takes a combined modelling and experimental approach.

CO_2 speciation in amine-based capture media

Understanding the speciation of the CO_2-rich capture medium is vital for understanding the catalytically active species for direct CO_2 electro-conversion in the capture medium. The mechanisms for CO_2 absorption in the amine-based capture medium have been widely studied.[38–40] This section discusses the evolution of the primary CO_2 species in the amine capture medium.

CO_2 loading effects

A typical amine scrubbing process (as shown in Fig. 1a) absorbs CO_2 from the post-combustion process using an aqueous alkanolamine solution, such as primary, secondary, and tertiary amines.[41] The benchmark amine that has been widely studied for CO_2 capture is monoethanolamine (MEA). In the absorption unit, CO_2 can react with primary amines to form carbamate ($RNHCO_2^-$) *via* the zwitterion mechanism at the first absorption stage (eqn (1)) and bicarbonate (HCO_3^-) ions at the second absorption stage (eqn (2) and (3)).[42] For tertiary amines, such as methyldiethanolamine (MDEA)[43,44] and 1-cyclohexylpiperidine (CHP) amine,[45] CO_2-amine reaction can only produce HCO_3^- as the primary product.[40] (eqn (4))

$$2RNH_2 + CO_2 \leftrightarrow RNHCO_2^- + RNH_3^+ \quad (1)$$

$$RHN_2 + CO_2 + H_2O \leftrightarrow HCO_3^- + RNH_3^+ \quad (2)$$

$$RNHCO_2^- + H^+ + H_2O \leftrightarrow HCO_3^- + RNH_3^+ \quad (3)$$

$$R_1R_2R_3N + CO_2 + H_2O \leftrightarrow R_1R_2R_3NH^+ + HCO_3^- \quad (4)$$

The product concentrations in CO_2-rich primary amines vary significantly with CO_2 loading. Aqueous MEA capture medium is a typical example,[46] as shown in Fig. 2. The MEA carbamate and protonated MEAs are the dominant products of CO_2 absorption when the CO_2 loading is below 0.4–0.5 mol_{CO_2}/mol_{amine}. (Fig. 2a) When the CO_2 loading increases further beyond 0.5 mol_{CO_2}/mol_{amine}, carbamate ions start to undergo hydrolysis to form bicarbonate ions (eqn (3)). At this stage, bicarbonate and freely dissolved CO_2 become the primary CO_2 species in the capture medium. Such speciation transformation with CO_2 loading usually takes place for primary (*e.g.*, MEA) and secondary amines such as diethanolamine (DEA),[46] as shown in Fig. 2b. In contrast, only bicarbonate concentration rises with the CO_2 loading in MDEA aqueous solution in tertiary amines (see Fig. 2c).[44]

In a typical CO_2 capture process using 20–30 wt% (equivalent to 3–5 M) aqueous MEA solution, the CO_2 loading is at 0.2–0.35 mol_{CO_2}/mol_{amine} for the CO_2-lean stream, and at 0.4–0.5 mol_{CO_2}/mol_{amine} for CO_2-rich stream.[47,48] These loadings indicate that: the carbamate is the dominant species at an estimated molar concentration of 1.7–2.5 M in the CO_2-rich MEA solutions. For secondary amines such as 40 wt% DEA, the typical CO_2 loadings are at similar levels to the MEA case, so the dominant products are carbamate ions. For tertiary amines such as MDEA solutions, the bicarbonate concentration is equivalent to CO_2 loading due to the dominant bicarbonate formation.

Temperature effects

Temperature serves a critical role in determining the CO_2-loading and speciation by affecting the solubility of CO_2 in amines and the equilibrium constants for multiple homogenous reactions. CO_2 solubility in the capture medium decreases with increasing temperatures, evident from the Henry constant relations with temperature shown in Fig. 3a.[49] Consequently, as implied in Fig. 3b, the CO_2 equilibrium partial pressure is higher for the CO_2-loaded MEA system at elevated temperatures.[50] Fig. 3b also shows that a high CO_2 loading lowers the heat of CO_2 absorption (which is an exothermic process), meaning that more CO_2 can be liberated from high-loading amines than low-loading ones.

The equilibrium constants (K) for the equilibrium reactions are governed by the enthalpy of the reaction (ΔH) and temperatures (T), as expressed in eqn (5). Fig. 3c suggested that the formation of bicarbonate ions from water and solvated CO_2 is promoted with increasing temperatures below 60 °C and is suppressed at a higher temperature. In Fig. 3d, the bicarbonate is prone to react with amines to form carbamate at lower temperatures for both MEA and DEA aqueous solutions.[51] The temperature governs the contents of the CO_2-related species in CO_2-rich amines and should profoundly impact the local speciation for the industrially relevant integrated electrolysers.

$$\frac{\partial \ln K}{\partial T} = \frac{\Delta H}{RT^2} \tag{5}$$

pH effects

Recent studies on gas-fed CO_2 electrolysis have shown that a more alkaline local reaction environment (pH > 10, see Fig. 4a)[52,53] close to the electrode surface than the electrolyte bulk due to the generation of the hydroxide ions from electroreduction reactions for both CO_2 and water (*i.e.*, hydrogen evolution reaction). The pH values in the capture medium usually change with the CO_2 loading. As an acidic gas, CO_2 usually acidifies the alkaline amine capture medium.[54] (Fig. 4b) A further reduction of the pH value by the absorbed CO_2 due to such acidification causes the second stage of the hydrolysis of the carbamate to bicarbonate, as described in eqn (3).[55] Additionally, a low pH value could reduce the energy required to recover CO_2 from the diluted amine solutions.[56] The pH can also swing back to alkaline conditions when the solvents are heated to separate CO_2 from the liquid. For high-rate CO_2 conversion in the amine capture medium, understanding the role of pH in regulating the homogenous amine reactions is important to study the reaction pathways for CO_2 delivery to the catalytically active sites and amine recovery.

The pH value of an amine solution is strongly correlated with the speciation. The pH usually swings between 8 and 10

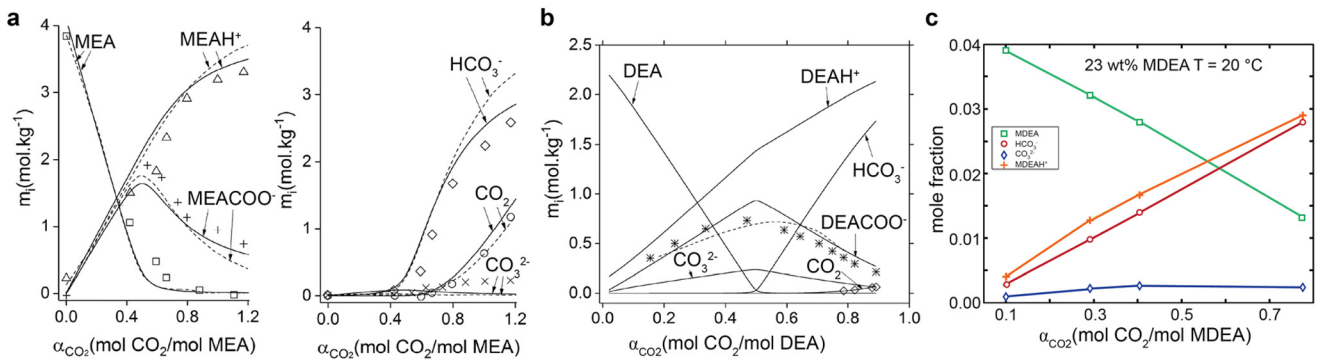

Fig. 2 Evolution of chemical species in the monoethanolamine-CO_2–H_2O system in (a) 20 wt% MEA at 40 °C, (b) 20 wt% DEA at 25 °C with symbols for experimental results and lines for calculated values (reproduced with permission,[46] Copyright 2018, American Chemical Society), (c) 23 wt% MDEA aqueous solution at 20 °C. Reproduced with permission.[44] Copyright 2005, American Chemical Society.

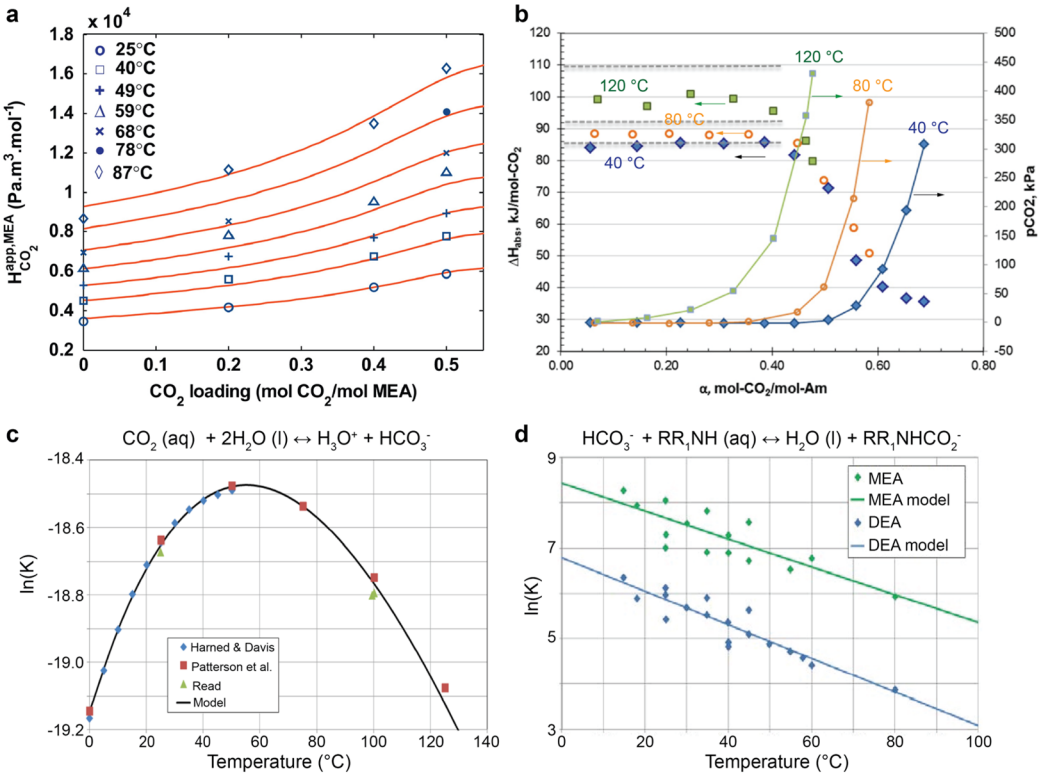

Fig. 3 The temperature effects on (a) Henry constant of CO_2, reproduced with permission,[49] copyright 2011, Elsevier. (b) CO_2 partial pressure and heat of CO_2 absorption for 30 wt% MEA aqueous solutions, reproduced with permission,[50] copyright 2014, Elsevier, (c) bicarbonate formation, and (d) carbamate formation for MEA and DEA aqueous solution. Reproduced with permission,[51] copyright 2017, Elsevier.

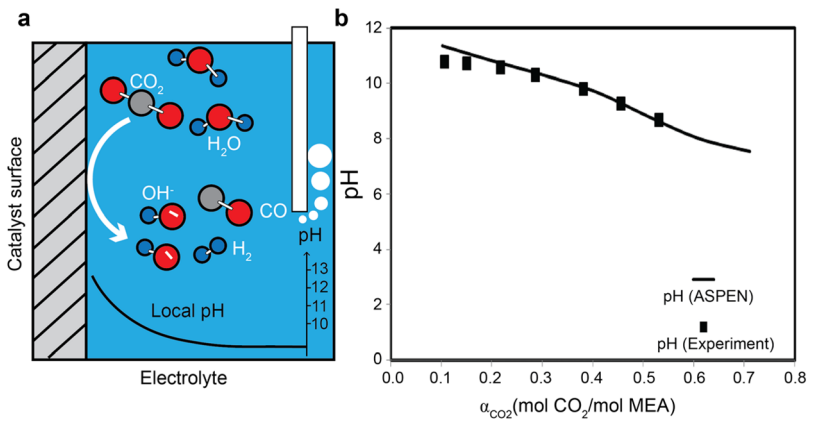

Fig. 4 (a) A schematic illustration of local pH difference for gas-fed CO_2 electroreduction close to the catalyst surface. (b) The pH evolution as a function of CO_2 loading in 30 wt% MEA aqueous solution at 21 °C. Reproduced with permission,[54] copyright 2012, American Chemical Society.

for CO_2 absorption and desorption cycle. In the MEA aqueous solution, for example, the bicarbonate formation and protonation of MEA take place at pH = ~6, CO_2 transformation to bicarbonate at pH = ~7, the carbonation from bicarbonate ions at pH = ~10.3, and deprotonation of $MEAH^+$ to MEA at a pH = ~10.[54]

These homogenous reactions could contribute to the recovery of the amines in the integrated electrolysers. By incorporating hydroxide ions into the system from electrochemical reactions, for example, one could expect the formation of free MEA and carbonates at the end equivalent points.[54] If added with protons from anode reactions and water electrochemical dissociation, the amine solution will end up with the formation of protonated amines and the evolution of gaseous CO_2.[54] Under electrochemical reduction conditions, it is likely that the solvent close to the catalyst surface experiences a much higher local pH than the bulk solution so that locally free amine tends to be regenerated and CO_2 species tend to form carbonate ions.

The recovery of amines and conversion of the absorbed CO_2 into valuable products take place either *via* electrochemical reactions or homogenous equilibrium reactions induced by the pH changes. Because the electrolyser is energy efficient when converting CO_2 to valuable product selectively, the recovery of the amines is desired to proceed with the reduction of absorbed CO_2 (*i.e.*, free dissolved CO_2, carbamate, and bicarbonate ions) and neutralisation of protonated amines inside the cathode channel, rather than electroreduction of protonated amines to hydrogen and amines. The locally produced carbonate ions, as a result of the raised local pH, should be reversed back to catalytically active species in the liquid bulk *via* reactions such as reacting with protons from the membrane to form CO_2 or carbamate.[55] In this case, we could envision that the recovery and recycling of the capture medium from the electrolyser requires dedicated control of the ion transport within the cell.

Catalytically active species for CO_2 electroreduction

As discussed in the section above, the carbamate, bicarbonate, and free dissolved CO_2 could contribute to the direct CO_2 electro-conversion in amine-based capture media because they are the primary species for the absorbed CO_2. Although there are limited direct findings for the underlying mechanisms for CO_2 conversion in amine capture media, we could explore the potential mechanisms by bringing the knowledge and mechanistic insights from the studies on gas-fed CO_2 electroreduction and direct bicarbonate reductions.[57] For gas-fed CO_2 electroreduction, freely dissolved CO_2 is widely deemed as the primary catalytically active reactant, no matter in a planar electrode (where CO_2 diffuses to the catalyst surface *via* the electrolyte bulk) or in gas-diffusion electrodes (where CO_2 diffuses to the catalyst surface *via* a hydrophobic porous matrix). In the direct bicarbonate reduction, where concentrated bicarbonate serves as the feed for CO_2 conversion, the evolved CO_2 molecules from acidification of bicarbonate are also recently unveiled as the actual primary active species for CO_2 conversion.[58,59] This section discusses recent reports focusing on the proposed mechanisms and active species for the integrated CO_2 conversion.

Free dissolved CO_2 as the active reactant

Unlike gas-fed CO_2 conversion and direct bicarbonate reduction, the CO_2-rich primary or secondary amines with a CO_2 loading below 0.5 mol_{CO_2}/ mol_{amine} has a negligible concentration of free dissolved CO_2 due to the carbamate formation. Such a low CO_2 concentration is usually considered the main cause for the observed lower conversion rates than in gas-fed scenarios. Chen *et al.*[60] claimed that the free dissolved CO_2 is the primary active reactant for MEA solution because they found that hydrogen evolution reaction dominates over smooth indium (In) and silver (Ag) foils for 30 wt% MEA aqueous solution with a CO_2 loading of 0.3, 0.4, and 0.48 mol_{CO_2}/mol_{MEA} in the presence of 0.1 wt% cetrimonium bromide (CTAB) surfactant. Such an independency between product faradaic efficiency and CO_2 loading indicates that the free dissolved CO_2 should serve as the primary active species, rather than the carbamate ions that should increase their concentrations with the CO_2 loading (see Fig. 2a). Similarly, Gallent *et al.*[61] also proposed that CO_2 needs to be liberated from amine solutions first before being reduced to different products. They confirmed their theory by demonstrating an enhancement of CO_2 conversion faradaic efficiency and rates over lead (Pb) or gold (Au) catalyst in CO_2-rich 1 M 2-amino-2-methyl-1-propanol (AMP) in propylene carbonate (PC) solutions. A similar mechanism was also proposed by Ahmad *et al.*,[62] who argued that the CO_2 liberated from AMP contributes to the CO_2 conversion.

In another report by Diaz *et al.*,[45] CHP was employed as the switchable polarity capture media for CO_2 conversion. This compound is a tertiary amine that is insoluble in water but can become soluble after reaction with CO_2 to produce bicarbonates and protonated amine. In this case, the bicarbonate becomes the primary CO_2 source. The authors used a proton-exchange membrane to promote protons produced from the anode chamber to release CO_2 from bicarbonate ions for the reaction. As a result, they detected a small amount of CO_2 in the product stream (see Fig. 5c), which experimentally confirms that CO_2 is released from the bicarbonate and contributes to CO production. In addition, Gallent *et al.*[61] reported a much more reduction in CO_2 loading (or more CO_2 liberated) at higher temperatures (75 °C *vs.* 15 °C) in 0.7 M tetraethylammonium chloride (TEACl) in PC solutions with 1 M AMP. (Fig. 5e) However, the CO_2 molecules converted are only up to 30% of the liberated CO_2. (see Fig. 5d and f) This comparison points to the essential role of released CO_2 as the active species for CO_2 conversion.

Because bicarbonate is the dominant product in the CO_2-loaded tertiary amine-based capture medium, the primary active reactant for conversion should be the free dissolved CO_2 from the acidification of bicarbonate. Therefore, as reported in recent work, CO_2 conversion in tertiary amine is anticipated to follow similar mechanisms for direct bicarbonate reduction.[57] Similar to direct bicarbonate reduction, CO_2 conversion in a bicarbonate-dominated CO_2-rich capture medium requires a supply of protons to produce CO_2 from bicarbonate ions. The proton flux is usually current-dependent and supplied from either anode reaction *via* a proton-exchange membrane[63,64] or the bipolar membrane[29,65,66] under a reversed bias. Protons could also cause an acidic local reaction environment close to the catalyst surface and contribute to the unwanted hydrogen evolution reaction.[67,68] Our recent two-phase one-dimensional model for direct bicarbonate reduction unveiled that the rate of CO evolution can be limited more by the formation and mass transfer of CO_2. Under high current densities, protons tend to either directly get reduced to hydrogen or react with the hydroxyls produced, so CO_2 regeneration and reduction pathways are limited.[68]

Carbamate as the active reactant

An alternative explanation for the observed low CO_2 conversion efficiency is the limited carbamate availability close to the cata-

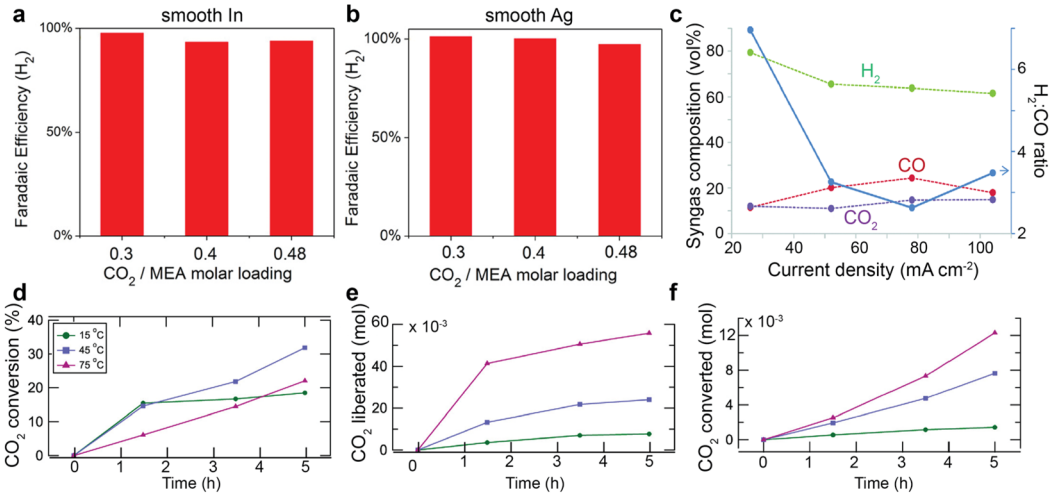

Fig. 5 Faradaic efficiency of H_2 over (a) smooth In and (b) smooth Ag surface in 30 wt% MEA aqueous solution loaded with 0.3, 0.4, 0.48 mol_{CO_2}/mol_{amine} in the presence of 0.1 wt% CTAB. Reproduced with permission,[60] copyright 2017, John Wiley and Sons. (c) Volumetric fractions of H_2, CO, and CO_2 as a function of current densities at 20 psig backpressure at Ag catalyst deposited on a reticulated vitreous carbon in CO_2 loaded CHP aqueous solution. Reproduced with permission,[45] copyright 2018, Royal Society of Chemistry. (d) The CO_2 conversion rate, the amount of (e) liberated CO_2 and (f) converted CO_2 as a function of time and temperatures. Reproduced with permission,[61] copyright 2021, American Chemical Society.

lyst surface due to the repulsion between the negatively charged carbamate anions and the negatively charged cathode. Lee *et al.*[37] explained the observed low CO faradaic efficiency from 2 M MEA aqueous electrolyte by the inefficient charge transfer between the cathode surface and the carbamate molecule. From the results of the electrochemical impedance analyses and *in situ* Raman spectroscopy, the authors proposed an interfacial electron transfer process, where the electron transfer must reach the carbamate ions through large $MEAH^+$ cations that are packed at the electrochemical double layer. The authors also showed that incorporating alkali cations such as K^+ helps achieve a more compact double layer with reduced availability of $MEAH^+$ and an improved CO faradaic efficiency.

Although the CO_2 species such as carbamate, bicarbonate, and free dissolved CO_2 should be the source for CO_2 reduction in the amine capture media, understanding the underlying mechanisms for CO_2 conversion remains unclear and needs further research efforts to detangle the complex electroreduction that involve multiple species, transport, and homogenous reactions. Generally, the reported performance for CO_2 electroreduction in amines is inferior to gas-fed conversion, which is usually explained by the low availability of reactants (either free dissolved CO_2 or negatively charged carbamate anions) close to the electrode surface. As compared to primary and secondary amines, it is more straightforward to understand the mechanisms for CO_2 reduction in tertiary amines by sourcing the knowledge and insights from the field of direct bicarbonate electro-reduction.

Strategies in achieving selective CO_2 conversion

Recent findings have shown that the catalysts that are selective for gas-fed CO electroreduction are also efficient for catalysis of CO_2 conversion in the amine capture media.[33,37,45,60,62,69,70] However, the performance of the integrated electrolyser is usually inferior to the state-of-the-art gas-fed electrolyser in terms of product faradaic efficiency, current densities, and cell potentials. Fig. 6a compares the energy performance of these two electrolysers to convert CO_2 to CO.[36] More importantly, recent studies demonstrate the potential to improve the faradaic efficiency and current densities for direct CO_2 conversion in an amine-based capture medium by tailoring the electrode structures, local reaction environment, and operating conditions such as temperatures and pressures, and cell design. A summary of achievements in recent studies is listed in Table 1.

A desired integrated CO_2 electroreduction should achieve a high current density with a high product faradaic efficiency at a low overpotential (*i.e.*, the excess of potential *vs.* the thermodynamic potential to drive the electrochemical reaction). Ideally, the amine as the electrolyte should exhibit a high ionic conductivity to minimise ohmic losses and reduce cell voltage. Fig. 6b from our recent energy analyses for CO_2-to-CO highlight the importance of product faradaic efficiency and cell potentials for the overall energy efficiency, where product faradaic efficiency serves a more critical role than cell potential.[36] Therefore, this section will review recent advances in improving the faradaic efficiency and current densities *via* electrode innovation and modification of the local reaction environment.

Ionic conductivity in amine solutions

The ionic conduction is essential for a complete electrochemical process. The ionic conductivity of the electrolyte (or capture medium) predetermines the ohmic loss, and thus has an impact on the overall cell potential.[1] However, amine capture media is poorly conductive as there are typically no added supporting ions, with ions only provided *via* CO_2

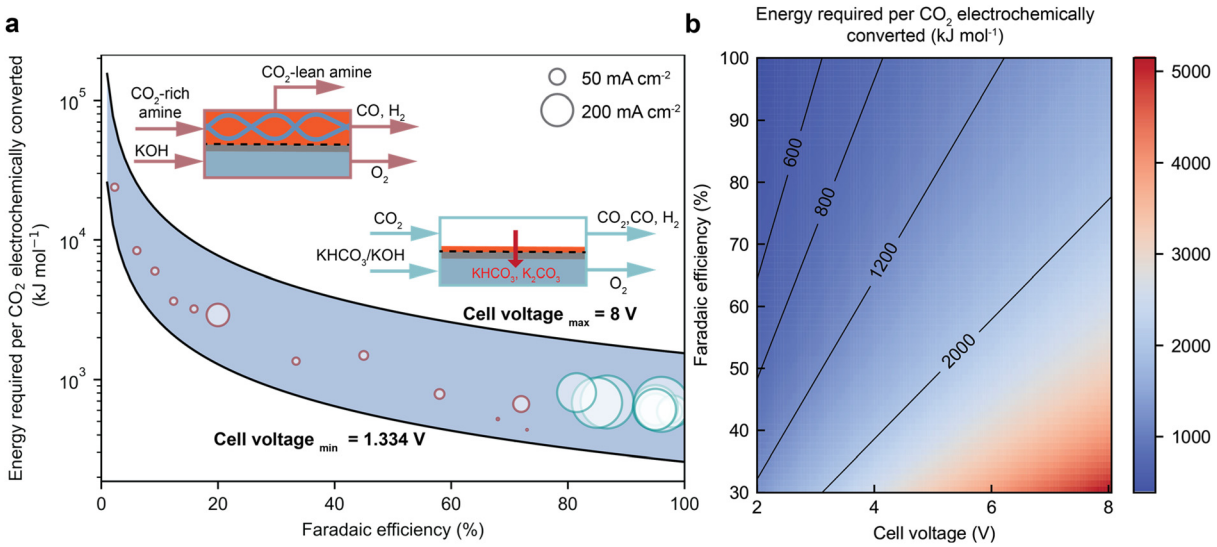

Fig. 6 (a) A comparison of the energy consumption, CO faradaic efficiency, and cell potentials over integrated and gas-fed CO_2 electrolysis. (b) The role of CO faradaic efficiency and cell voltage in determining the overall energy consumption of CO_2 electrolysis to produce CO.[36]

Table 1 A summary of recent studies data for CO_2 electroreduction in amine-based capture media

Cathode	Cathode Potential (V) *vs.* RHE	Product	Peak $FE_{product}$ (%)	Current densities at peak $FE_{product}$ (mA cm^{-2})	Solvents and conditions	Ref.
Ag/carbon-black on 300 nm Ag film on ePTFE	−0.8	CO	72	50	30 wt% MEA aqueous solution mixed with 2M KCl at 60 °C	37
Ag/carbon-black on 300 nm Ag film on ePTFE	−1.2	CO	20	100		
Smooth Ag	−0.8	CO	12.4	—	30 wt% MEA aqueous solution at 22 °C	60
Smooth Bi	−0.8	Formate	35.7	—		
Porous Ag	−0.8	CO	39.1	—		
Smooth Ag	−0.8	CO	33.4	—	30 wt% MEA aqueous solution with	
Smooth In	−0.8	Formate	45.4	—	0.1 wt% CTAB loaded with CO_2 at 22°	
Smooth Sn	−0.8	Formate	19	—		
Porous In	−0.8	Formate	54.5	—		
Porous Pb	−0.8	Formate	60.8	—		
Porous Ag	−0.8	CO	38.2	—		
Cu	−0.78	CO	45	18.4	0.1 mM ethylenediamine carbamate in 0.1 M $NaClO_4$ saturated with CO_2	71
Smooth Au foil	−1.9 *vs.* Ag|AgCl	CO	~45	~15	1 M 2-amino-2-methyl-1-propanol (AMP) and propylene carbonate (PC) solution	61
Pb electrode	−2.5 *vs.* Ag|AgCl	Formate	~40	~28	2 M AMP in PC solution at 75 °C	
HCl treated Ag foil	−0.91−−1.01	CO	91 ± 7	~10	0.25–1 M AMP aqueous solution at room temperature with 0.3 mM CTAB saturated with CO_2	62
Ag foil	−0.91	CO	72 ± 8	~11	1 M AMP aqueous solution	
Au/MgAl-LDHs	−0.4	CO	~68	~1.1	1.0 M alcohol amine solution	72
Cu/MgAl-LDHs	−0.25	CO	~73	~0.5	(*n*(ethanolamine): *n*(diethanolamine) = 2 : 3)	
Ag	−1.1	CO	71	15	[MEAHCl][MDEA], where MEAHCl is ethanolamine hydrochloride, and MDEA is methyl diethanolamine	73
Au nano dendrites	−1.0	Formate	60.3[a]	~46	0.05 M MEA aqueous solution	74
Ag microparticles mixed with Nafion and PTFE deposited on a reticulated vitreous carbon	—	CO	~30	78	1-Cyclohexylpiperidine aqueous solution with 0.2 M K_2SO_4 loaded with CO_2 with back pressure of 20 psig	45
Ni-N-C single-atom-catalyst	−0.6	CO	63.2	~4	CO_2-rich 5 M MEA solution	75

[a] Current efficiency calculated from $(j_{CO_2} - j_{Ar})/j_{CO_2}$, where j is the current density, and the current densities were collected in the presence of the subscript gases.

absorption. Taking MEA aqueous solution as an example,[76] as shown in Fig. 7a and b, CO_2 absorption causes an increase in ionic conductivity of the capture medium because the CO_2 reactions increase the availability of ions (such as carbamate anions, bicarbonate anions, and $MEAH^+$) as charge carriers for ion conduction. Fig. 7b shows that 3–4 M of MEA could be an optimal concentration range for the highest ionic conduction. However, even the highest conductivity (~40 mS cm^{-1}) for CO_2-saturated MEA solution is not comparable to the ionic conductivity of 1 M KOH (215 mS cm^{-1}).[77] Such a trend remains valid for the CHP-CO_2–H_2O system shown in Fig. 7c. The ionic conductivity peaks at the CHP-H_2CO_3 concentration of ~1.2 M and then drops with a further increase in the concentration. In contrast, in the system added with 0.2 M K_2SO_4, the overall ionic conductivity nearly doubles the ionic conductivity for bare CHP-H_2CO_3 at diluted conditions but also decreases with the concentration of CHP-H_2CO_3.[45]

Electrode materials and structures

The electrode for the integrated CO_2 conversion is desired to provide a high density of the electrochemically active sites with high catalytic activity. A few studies performed similar techniques used for gas-fed CO_2 electroreduction to deposit catalyst nanoparticles (*e.g.*, Ag) onto a substrate such as reticulated vitreous carbon foam or gas-diffusion layer (made from carbon or polytetrafluoroethylene (PTFE)) *via* coating (*e.g.*, spray coating) and sputter deposition techniques, which are commonly used for electrode preparation for gas-fed CO_2 electroreduction. (see Fig. 8a) For example, Lee *et al.* prepared their Ag electrodes by first sputtering ~300 nm Ag film on the PTFE porous membrane and then spraying Ag nanoparticles and carbon black on top of the sputtered Ag film. Such an electrode can achieve 50 mA cm^{-2} with a CO faradaic efficiency of about 72% at −0.8 V *vs.* reversible hydrogen electrode (RHE). In another recent report, Ahmad *et al.*[73] boosted the CO faradaic efficiency of CO up to ~91% in 0.25–1 M CO_2-saturated AMP aqueous solution with 0.3 mM CTAB by treating Ag foils with HCl. More recently, Kim *et al.*[75] showed that applying nickel (Ni) single-atom catalyst as shown in Fig. 8b on a gas-diffusion electrode can achieve 64.9% CO faradaic efficiency from 5 M MEA aqueous solution at 50 mA cm^{-2} in a membrane electrode assembly.

The requirement for the electrode structure for integrated electrolysis should be different from the gas-diffusion electrode used for gas-fed CO_2 reduction due to the absence of CO_2 supply in the integrated electrolysers.[80–82] Therefore, a highly hydrophilic electrode surface should help improve its contact with solvent and minimise the contact with the gas product. Most metallic electrodes are hydrophilic, and their hydrophilicity is anticipated to increase if the electrode surface is roughened according to the Wenzel equation[83] and under electric potential due to the electrowetting phenomenon.[80]

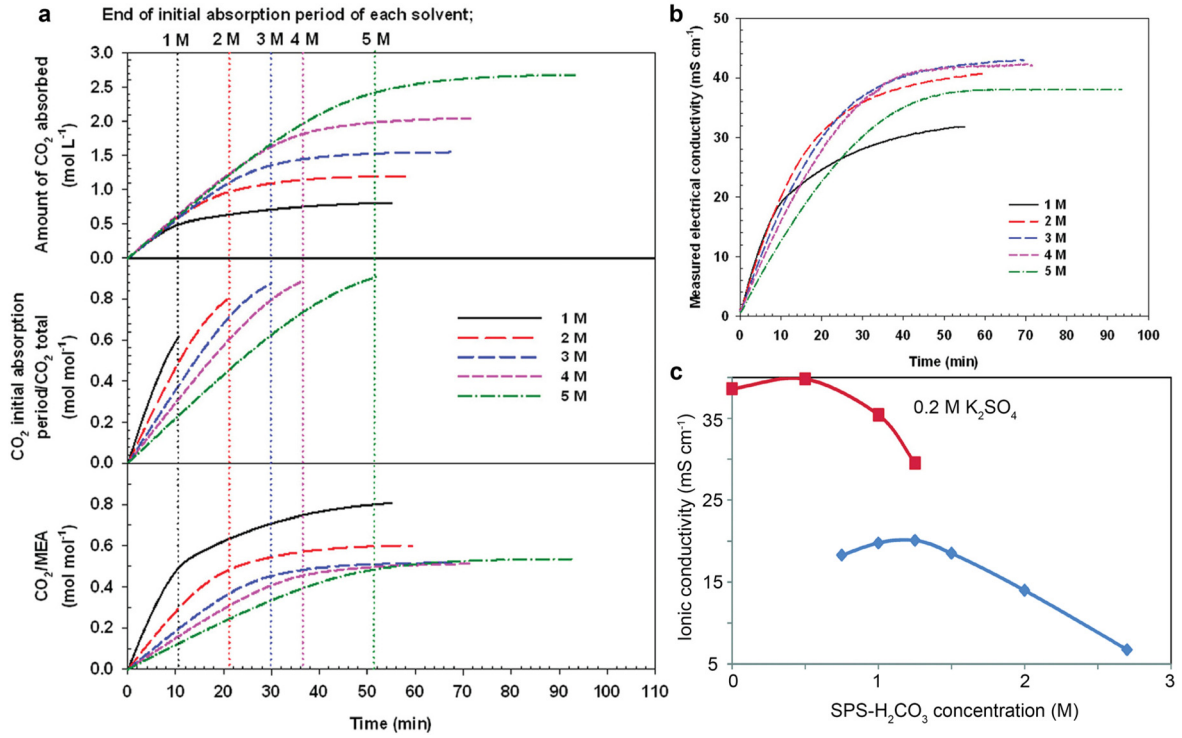

Fig. 7 (a) The CO_2 absorption amount, molar ratio, and CO_2/MEA ratio as a function of time at different MEA concentrations. (b) The electrical conductivity of the MEA aqueous solutions with different concentrations as a function of CO_2 absorption durations. Reproduced with permission,[76] copyright 2016, American Chemical Society. (c) The ionic conductivity of CO_2 loaded CHP aqueous solution with and without 0.2 M K_2SO_4 as a function of amine concentration. Reproduced with permission,[45] copyright 2017, Royal Society of Chemistry.

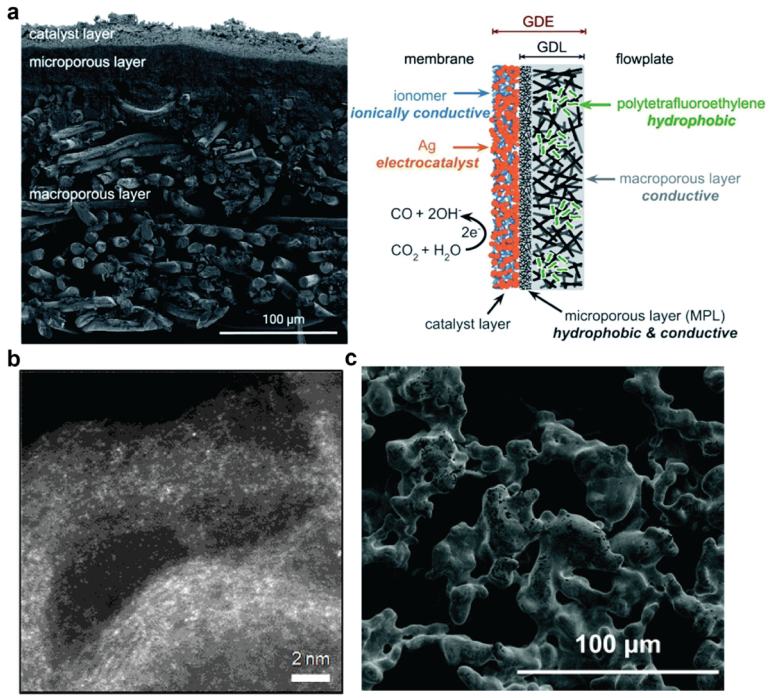

Fig. 8 (a) A scanning electron micrograph of the cross-section (left panel) and illustration (right panel) for a gas-diffusion electrode. Reproduced with permission,[78] copyright 2020, American Chemical Society. (b) A high-angle annular dark-field transmission electron micrograph of the Ni-nitrogen–carbon single-atom catalyst. Reproduced with permission,[75] CC BY 4.0 License. (c) A scanning electron micrograph of the porous silver metal electrode for direct bicarbonate reduction. Reproduced with permission,[79] copyright 2022, Royal Society of Chemistry.

Compared to the development of the gas-diffusion electrodes, the requirement for the electrode development is less stringent on maintaining a stable wetting condition and gas–liquid interfaces within the electrode.[75,80,84,85] In the field of direct bicarbonate reduction, for example, when the Berlinguette group directly incorporated Ag foam instead of carbon-based Ag gas-diffusion electrodes, the bicarbonate electrolyser can achieve a further improvement of the performance.[79,86]

As bicarbonate is the main source of CO_2 reduction in tertiary amines, we could also apply the advances in the development of direct bicarbonate reduction to improve the performance further. Although direct bicarbonate reduction is outside the scope of this review, we reckon it is worth mentioning an example reported by Zhang *et al.*[79] They demonstrated that the gas diffusion layer without a microporous layer and PTFE showed the best performance during direct bicarbonate reduction.[78] Furthermore, the same group developed new electrodes to enhance CO_2 electroreduction to CO in a 3 M bicarbonate aqueous solution. They showed that a porous Ag electrode (see Fig. 8c) is superior to the Ag-based gas-diffusion electrodes in evolving CO from bicarbonate solutions, especially at current densities >100 mA cm^{-2}.[63] These findings confirm that a hydrophilic porous electrode is likely applicable to CO_2 conversion in the tertiary amines than electrode structures used in gas-fed electrolysis.

A few studies reported that applying porous electrodes can improve product faradaic efficiency. For example, Chen *et al.*[60] prepared a few porous electrode structures based on metals, such as Ag, zinc (Zn) and Indium (In), using the hydrogen-bubble templated electrodeposition technique. The microstructures of some porous electrodes are shown in Fig. 9a. The authors observed an enhancement of formate production over porous In and CO production over Zn and Ag porous electrodes in a CO_2-saturated 30 wt% MEA aqueous solution. Therefore, the porous microstructure could be beneficial for CO_2 conversion. In another example, Hossain *et al.*[74] prepared nano dendrites based on Cu, gold (Au), and Ag by growing the metals on a glassy carbon *via* a galvanic replacement reaction in the mixed solution of metal precursors and Zn dust. (see Fig. 9b) From a more significant increment of current densities in argon- *versus* CO_2-saturated 0.05 M MEA aqueous solutions, the authors concluded that the nanostructured catalyst could improve CO_2 conversion current densities and charge-transfer efficiency.

Local reaction environment

In addition to the electrode, a local reaction environment close to the catalyst surface is essential to provide sufficient reactants and suppress unwanted side reactions such as hydrogen evolution reactions. As mentioned earlier, the local chemical speciation could vary vastly with the amines,[61,71,75] CO_2 loading,[60] local pH, proton supply,[45,75] alkali cations,[37,69,75] temperatures,[37,61] and electrochemical operating conditions.[62] An ideal local reaction environment should maintain sufficient catalytically active species, minimise surface coverage of protonated amines and protons that leads to hydrogen

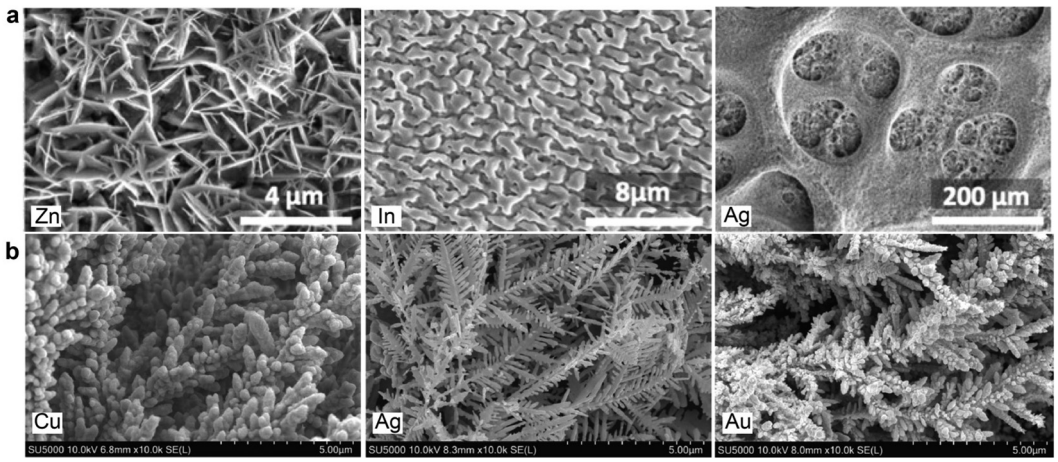

Fig. 9 Scanning electron micrographs of (a) porous Zn, In, and Ag electrodes prepared by hydrogen-bubble-templated electrodeposition technique, reproduced with permission,[60] copyright 2017, John Wiley and Sons. (b) Cu, Ag, and Au nano dendrites on glassy carbon prepared *via* galvanic replacement reaction. Reproduced with permission,[74] copyright 2020, John Wiley and Sons.

formation, facilitate fast ion conduction and charge transfer, and provide a benign environment for amine recovery.

A straightforward strategy to modify the local reaction environment is to change the types and concentrations of the amines, which predetermine the CO_2 species and their concentration in the solvent bulk and thus in the local reaction environment. In the previous sections, we have discussed some examples showing that the product Faraday efficiencies are different in MEA solutions and CHP solutions. In addition, Abdinejad *et al.*[71] reported different product distribution over Cu electrode in 0.1 M $NaClO_4$ solution containing carbamate from MEA, ethylenediamine (EDA), and decylamine (DCA). As shown in Fig. 10a. The EDA-containing electrolyte achieved the highest CO faradaic efficiency among the tested amines, likely due to its two primary amines in one EDA molecule. Another report by Gallent *et al.*[61] shows that 2 M AMP in PC solution is the optimal concentration to convert CO_2 to formate at the highest faradaic efficiency and reaction rates, but leads to the lowest overall current densities over lead (Pb) electrode. (Fig. 10b) Similarly, Ahmad *et al.*[62] also report that the optimal AMP concentration is within 0.25–1 M for CO production over HCl-treated Ag electrode.

A few studies[37,62,69] drew consistent conclusions that the addition of alkali salts can improve product selectivity mainly due to the presence of large alkali cations (*e.g.*, K^+ or Cs^+), while anions show negligible effects on the CO_2 conversion. In brief, large alkali cations are reported to promote CO_2 conversions in amines *via* multiple benefits, such as (i) enhancing charge transfer from the electrode to carbamate,[37] (ii) facilitating fast ion pairing with carbamate,[69] (iii) destabilising the formation of carbamate hence facilitating carbon–oxygen bond cleavage,[69] (iv) suppressing hydrogen evolution reaction, (v)

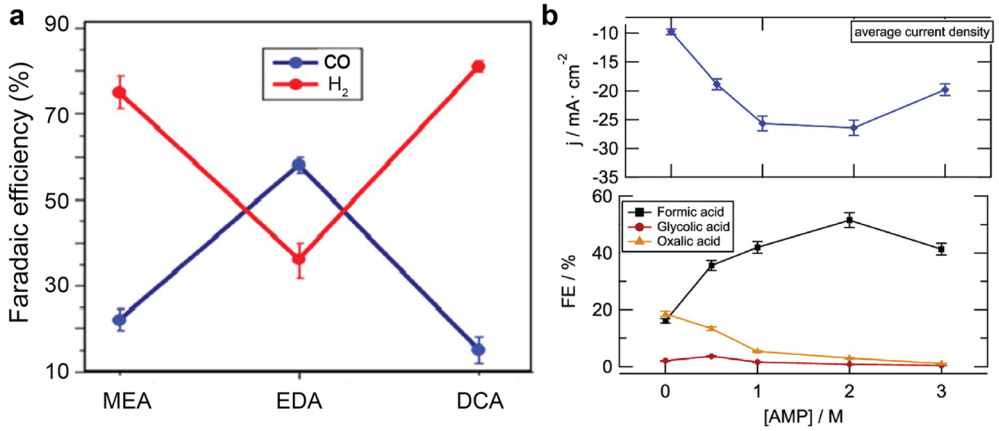

Fig. 10 (a) Faradaic efficiency of CO and H_2 over Cu catalyst in 0.1 M $NaClO_4$ solution with MEA, ethylenediamine (EDA), and decylamine (DCA) at −0.78 V *vs.* RHE. Reproduced with permission,[71] copyright 2020, American Chemical Society. (b) The change of current densities and product faradaic efficiency over Pb electrode as a function of 2-amino-2-methyl-1-propanol (AMP) in propylene carbonate solutions at −2.5 V *vs.* Ag|AgCl at 75 °C. Reproduced with permission,[61] copyright 2021, American Chemical Society.

strengthening local electrified field[87] (for free dissolved CO_2), and (vi) stabilising key reaction intermediates.[88,89]

When CO_2 serves as the active species for CO_2 conversion, according to recent reports,[88,90–92] cations play a crucial role in activating CO_2 electroreduction in the CO_2-gas-fed system, rather than modifying local electric field or buffering local pH. The findings from Monteiro's report[88] show that weakly hydrated cations (*e.g.*, Cs^+ and K^+) can be concentrated at the catalyst surface and tend to stabilise the negatively charged intermediates (*e.g.*, $*CO_2^-$) *via* a local electric field effect, including medium-range electric field-dipole interaction and short-range electrostatic interaction. In the case of the integrated electrolysis, Lee *et al.*[37] observed an improvement of CO faradaic efficiency in MEA solutions with Cs^+ cations as compared to K^+ cations. An earlier report also unveiled that the large alkali cations weaken carbamate formation and promote CO_2 reduction current densities for CO_2-loaded 0.1 M 2-ethoxyethylamine (EEA) in dimethyl sulfoxide (DMSO).[69] In their CO_2-EEA-DMSO system, the primary product is carbamic acid if there are no salts added. In contrast, the primary product distribution shifts towards a more significant proportion of carbamate ions with alkali cations following the order K^+ < Na^+ < Li^+ (see Fig. 11a). Density functional theory (DFT) calculations suggest that the large alkali cations weaken the C–N bond and increase O–C–O bond angles due to low inductive effects between $-COO^-$ and the soft Lewis acids. Despite the low availability of carbamate ions, K^+ cations achieve the highest current densities among other small cations. Their molecular dynamics (MD) simulation results, as shown in Fig. 11b, point out that the improvement could be correlated with an easier desolvation and more rapid pairing kinetics with carbamate over K^+ than over Li^+.

Interestingly, Kim *et al.*[75] report that the effects of cations vary with the catalyst types: Ni single-atom catalyst is less sensitive to cation effects than a metallic catalyst. The authors attributed such trend to the high potential of zero charges of single-atom catalysts that can maintain a high surface charge density no matter the size of the alkali cations. In addition, Ni single-atom catalyst is considered a unique catalyst that has a weak binding with protons and poor kinetics to evolve hydrogen during gas-fed CO_2 electrolysis.[70,93] The suppression of hydrogen evolution reaction for Ni single-atom catalyst could contribute to the observed insensitivity of the catalyst to alkali cations.

Further, the side hydrogen evolution reaction during CO_2 electroreduction in amines can be suppressed by incorporating surfactant in the solvents. The results shown in Fig. 12, as reported by Chen *et al.*,[60] suggest the cation surfactant (*i.e.*,

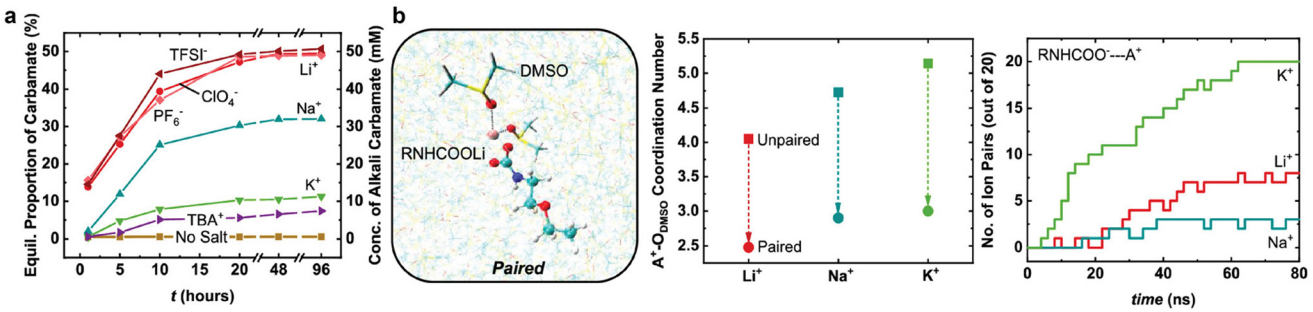

Fig. 11 (a) Comparison of equilibrium population and concentration of alkali and tetrabutylammonium (TBA^+) cations in CO_2 -loaded 0.1 M EEA in DMSO. (b) A Li-carbamate pairing configuration solvated in DMSO (left) and molecular dynamics simulations results in alkali cations coordination numbers (middle) and the number of ion pairs formed against computation time (right). Reproduced with permission,[69] copyright 2019, American Chemical Society.

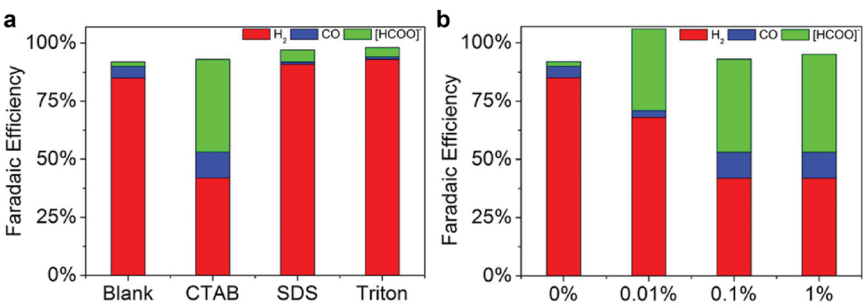

Fig. 12 Product distributions of CO_2 reduction over indium catalyst at −0.8 V *vs.* RHE in CO_2-saturated 30 wt% MEA aqueous solution with (a) 0.1 wt% of CTAB, sodium dodecyl sulfate (SDS), and Triton surfactants, and (b) with different concentrations of CTAB surfactant. Reproduced with permission,[60] copyright 2017, John Wiley and Sons.

CTAB) can boost the CO_2 conversion to formate and CO, while anion surfactant (*i.e.*, sodium dodecyl sulfate) only improve the selectivity towards formate. In contrast, there is no noticeable improvement when Triton surfactant is present in the solution. The authors also observed a lower current density in the presence of CTAB surfactant, which is an indication that the CTAB enhance the CO_2 conversion selectivity mainly *via* the suppression of hydrogen evolution reaction. Therefore, the beneficial effect of these additives is different from the cation effect. Including cation mainly promotes CO_2 conversion, while including these additives could alter proton availability and proton reduction activity.

As shown in Fig. 12b, additionally, the content of the CTAB surfactant also has a profound impact on the product distribution. A high content (>0.1 wt%) of CTAB is helpful in promoting CO, and a low content (0.01 wt%) is sufficient to improve the formate production. If combined with the porous indium electrode, one could achieve a formate faradaic efficiency of 45.4% and a CO of 17.0% in 30 wt% MEA aqueous solution. Similar beneficial effects of the CTAB are also reported for quaternary ammonium compounds for gas-fed CO_2 electroreduction,[94–97] highlighting the similarity of mechanisms between integrated and gas-fed electrolysis. The observed faradaic-efficiency overshoot in Fig. 12b could be a result of the mismatch of the effluent flow rate, current densities, and gas concentration while calculating the faradaic efficiency. This issue takes place when the reaction system does not reach a steady state, which is sometimes challenging to achieve experimentally and adds complexity to the measurement of the performance for CO_2 electrolysis.

Temperatures and pressures

As mentioned previously, temperature is an important factor in determining the chemical speciation in the capture medium. An elevated temperature normally shifts the reaction equilibrium towards the evolution of CO_2 from the capture medium (see Fig. 3a and b) but decreases CO_2 solubility in water. On the electrochemical reaction side, due to the Joule heating, the local temperature at the catalytic interface is generally higher than the solvent bulk, especially when the electrolyser is at high current densities.[98] High operating temperatures could also accelerate the mass transport and reaction kinetics for both CO_2 conversion and side hydrogen evolution reaction. Tailoring the operating temperature could be an effective strategy to enhance the current densities and product selectivity.

By lifting the operating temperature up to 60 °C, Lee *et al.*[37] demonstrated the feasibility of achieving 50 mA cm^{-2} with 72% CO faradaic efficiency over Ag gas-diffusion electrode in a flow cell system fed with 2 M MEA solution. Fig. 5f also shows another impact of temperature on CO_2 conversion. Elevated temperatures (*e.g.*, 75 °C) can enhance the rate of CO_2 conversion over Pb for the CO_2-AMP-PC system but may leave too much liberated CO_2 unreacted before leaving the system.[61] Therefore, a moderate temperature is beneficial to achieve a relatively high conversion rate and CO_2 conversion efficiency. Similarly, Kim *et al.*[75] also observed that the CO partial current densities reach peak values when the temperature is moderate (40 °C *vs.* 60 °C) in 5 M MEA aqueous solutions.

The pressure is another important factor that affects the dissolved CO_2 in the capture medium. High pressure at cathode chamber increases CO_2 solubility in the solvents and enhances the concentration of the free dissolved CO_2 in the solvent. Diaz *et al.*[45] reported a promoted CO faradaic efficiency (2.9%) when there is a back pressure of 20 psig compared to the faradaic efficiency (1.1%) without backpressure in CHP. Further increase in back pressure to 40 psig can improve CO faradaic efficiency by 20% at about 104 mA cm^{-2}. These results highlight the importance of reporting the backpressure at the cathode side for CO_2 conversion in the capture medium. Increasing the pressure of the CO_2-loaded liquid is also effective in improving CO selectivity from bicarbonate reduction.[79]

Cell configuration

The cell configuration design also matters to achieve an optimal CO_2 conversion rate from amines. As the active species, products, and recovered amines need to transport between solvent bulk and the electrode surface. Such configuration is similar to the scenario in CO_2 transport within an H-cell configuration, where there is a thick hydrodynamic layer about 40–120 μm in thickness.[99,100] Such a thick hydrodynamic boundary layer could slow down the local mass transfer of reactants, products, and ions. The flow cell configuration reported by Lee *et al.*[37] partially contributed to the enhancement of CO_2 conversion rate in amines. Flow cells allow the solvent to continuously flow in and out within the cell and can help reduce the reduce the thickness of the stagnant film. In addition, membrane electrode assembly is another promising configuration (see Fig. 1c), where there is no gap between electrodes (both cathode and anode) and membrane. Such configuration can further reduce ohmic loss arising from electrolyte ion conduction. Kim *et al.*[75] employed such cell configuration and significantly improved the rates of CO_2 conversion. Similarly, Zhang *et al.*[79] demonstrated that a membrane electrode assembly with porous flow-through the electrode could also boost the overall CO_2 conversion selectivity at industrially relevant rates from concentrated bicarbonate solutions. If the primary reactant is bicarbonate ions, the cell should allow sufficient CO_2 liberation from bicarbonate by supplying protons and accelerating concentrated free dissolved CO_2 locally at the catalyst surface.[68] Employment of proton-conducting membrane[45] or bipolar membrane[75] could ensure the proton supply to the solvents. Modelling studies[67,68] have shown that by adjusting the thickness, porosity and permeability of the catalyst layer, together with the thickness and ion transport activity of the cation membrane or bipolar membrane, bicarbonate electrolysers can reach higher activity and selectivity under lower cell voltages.

Conclusions and outlook

In conclusion, integrating CO_2 capture based on amine scrubbing and electrochemical conversion has the potential to reduce the overall capital and operational cost further. The critical enabler is the development of energy-efficient integrated CO_2 electroreduction that can convert the absorbed CO_2 to valuable products and regenerate amines simultaneously. However, CO_2-amine solution could be a complex system involving multiple homogeneous equilibrium reactions, which are determined by factors such as CO_2 loading, temperatures, pressures and pH. The catalytic interface for CO_2 conversion usually shows a much higher pH and temperature than the solvent bulk during high-rate electrolysis, which could affect the chemical speciation. Although the catalytically active species for CO_2 electroreduction is under debate, these species should certainly come from carbamate, bicarbonate, and free dissolved CO_2. Free dissolved CO_2 molecules are the active species for the latter two. All these species are found limited close to the catalyst surface, particularly at high current densities, mainly due to either limited liberation of CO_2, slow transport of CO_2, or electrostatic repulsion. Recent studies also demonstrated exciting improvements in CO_2 conversion and suppression of side reactions by innovating electrode structures and catalysts, optimising the local reaction environment (amine types, amine content, alkali cations), increasing pressures and temperatures, and designing cell configurations.

Further research efforts are demanded to address challenges in advancing integrated electrolysis. First, it remains unclear about the dominant active reactant for CO_2 conversion in the capture media, but the understanding of the active species is essential for the future rational design of the catalytic interfaces and systems. It is possible to take advantage of *operando* or *in situ* spectroscopy technology, such as attenuated total reflectance – surface-enhanced infrared absorption spectroscopy (ATR – SEIRAS), Raman spectroscopy, and mass spectroscopy, to probe the local reaction environment and products under electrochemical conditions. In addition, multiscale theoretical calculations such as DFT, MD, and multiphysics modelling and simulation could help provide insights into the reaction mechanisms and local reaction environment. The new knowledge generated from these investigations can also guide us in designing the next generation of integrated electrolysis through the choice of the capture medium, modulation of ion transport, electrocatalyst and electrode structure design, process optimisation and cell configuration innovation.

The electrocatalysts and electrode structures in recent reports are similar to the electrodes used in gas-fed CO_2 reduction. However, the electrode is desired to be more hydrophilic for the integrated electrolysis to increase electrochemically active surface area and minimise gas-electrode contact, which is different from the gas-fed reaction that requires a stable combination of the hydrophobic and hydrophilic surface. Therefore, further electrode development could explore the hydrophilic porous electrode, such as porous metallic films, allowing the solvent to flow within the electrode structure.

Furthermore, the cell configuration is another key contributor to the overall performance of the integrated electrolysers because it determines the conditions of the reaction zones for homogeneous reactions, such as the liberation of CO_2 through bicarbonate acidification and ion transportation. Additional research is urgently needed to understand the compatibility between the CO_2-rich amines and ion-exchange membranes. More modelling work could also help understand the role of cell dimensions in determining flow dynamics, CO_2 liberation, and ion conduction.

Finally, both CO_2 capture and electrolysis are fast-growing fields. It is essential to keep evaluating the technical and economic viability of both sequential and integrated pathways. The advancement of materials, processes, and techniques in both fields could contribute to the improvement of the integrated electrolysis and further cost reduction for CO_2 capture and utilisation.

Conflicts of interest

We declare no conflicts of interest.

Acknowledgements

C. Z. acknowledges the support by Australian Research Council (FT170100224).

References

1 S. Garg, M. Li, A. Z. Weber, L. Ge, L. Li, V. Rudolph, G. Wang and T. E. Rufford, *J. Mater. Chem. A*, 2020, **8**, 1511–1544.
2 D. Wakerley, S. Lamaison, J. Wicks, A. Clemens, J. Feaster, D. Corral, S. A. Jaffer, A. Sarkar, M. Fontecave, E. B. Duoss, S. Baker, E. H. Sargent, T. F. Jaramillo and C. Hahn, *Nat. Energy*, 2022, **7**, 130–143.
3 H. Shin, K. U. Hansen and F. Jiao, *Nat. Sustain.*, 2021, **4**, 911–919.
4 P. D. Luna, C. Hahn, D. Higgins, S. A. Jaffer, T. F. Jaramillo and E. H. Sargent, *Science*, 2019, **364**, eaav3506.
5 F. P. G. d. Arquer, C.-T. Dinh, A. Ozden, J. Wicks, C. McCallum, A. R. Kirmani, D.-H. Nam, C. Gabardo, A. Seifitokaldani, X. Wang, Y. C. Li, F. Li, J. Edwards, L. J. Richter, S. J. Thorpe, D. Sinton and E. H. Sargent, *Science*, 2020, **367**, 661–666.
6 J. E. Huang, F. Li, A. Ozden, A. S. Rasouli, F. P. G. d. Arquer, S. Liu, S. Zhang, M. Luo, X. Wang, Y. Lum, Y. Xu, K. Bertens, R. K. Miao, C.-T. Dinh, D. Sinton and E. H. Sargent, *Science*, 2021, **372**, 1074–1078.

7 B. Endrődi, A. Samu, E. Kecsenovity, T. Halmágyi, D. Sebők and C. Janáky, *Nat. Energy*, 2021, **6**, 439–448.
8 P. Grammelis, N. Margaritis and E. Karampinis, in *Fuel Flexible Energy Generation*, ed. J. Oakey, Woodhead Publishing, Boston, 2016, pp. 29–58, DOI: **10.1016/B978-1-78242-378-2.00002-X**.
9 J.-M. G. Amann and C. Bouallou, *Energy Procedia*, 2009, **1**, 909–916.
10 X. Wang and C. Song, *Front. Energy Res.*, 2020, **8**, DOI: **10.3389/fenrg.2020.560849**.
11 C. J. o. C. Engineering, M. Abdinejad, C. Dao, B. Deng, F. Dinic, O. Voznyy, X.-a. Zhang and H.-B. Kraatz, *ACS Sustainable Chem. Eng.*, 2020, **8**, 9549–9557.
12 M. Abdinejad, A. Seifitokaldani, C. Dao, E. H. Sargent, X.-a. Zhang and H. B. Kraatz, *ACS Appl. Energy Mater.*, 2019, **2**, 1330–1335.
13 M. Abdinejad, K. Tang, C. Dao, S. Saedy and T. Burdyny, *J. Mater. Chem. A*, 2022, **10**, 7626–7636.
14 M. Abdinejad, C. Dao, X.-A. Zhang and H. B. Kraatz, *J. Energy Chem.*, 2021, **58**, 162–169.
15 M. Li, X. Tian, S. Garg, T. E. Rufford, P. Zhao, Y. Wu, A. J. Yago, L. Ge, V. Rudolph and G. Wang, *ACS Appl. Mater. Interfaces*, 2020, **12**, 22760–22770.
16 M. Li, M. N. Idros, Y. Wu, S. Garg, S. Gao, R. Lin, H. Rabiee, Z. Li, L. Ge, T. E. Rufford, Z. Zhu, L. Li and G. Wang, *React. Chem. Eng.*, 2021, **6**, 345–352.
17 M. Sassenburg, R. de Rooij, N. T. Nesbitt, R. Kas, S. Chandrashekar, N. J. Firet, K. Yang, K. Liu, M. A. Blommaert, M. Kolen, D. Ripepi, W. A. Smith and T. Burdyny, *ACS Appl. Energy Mater.*, 2022, **5**, 5983–5994.
18 K. Liu, W. A. Smith and T. Burdyny, *ACS Energy Lett.*, 2019, **4**, 639–643.
19 M. Abdinejad, I. S. d. Silva and H. B. Kraatz, *J. Mater. Chem. A*, 2021, **9**, 9791–9797.
20 H. Liu, S. Cao, L. Chen, K. Zhao, C. Wang, M. Li, S. Shen, W. Wang and L. Ge, *Chem. Eng. J.*, 2022, **433**, 133594.
21 M. Abdinejad, E. Irtem, A. Farzi, M. Sassenburg, S. Subramanian, H. P. I. v. Montfort, D. Ripepi, M. Li, J. Middelkoop, A. Seifitokaldani and T. Burdyny, *ACS Catal.*, 2022, **12**, 7862–7876.
22 W. A. Smith, T. Burdyny, D. A. Vermaas and H. Geerlings, *Joule*, 2019, **3**, 1822–1834.
23 D. Cebrucean, V. Cebrucean and I. Ionel, *Energy Procedia*, 2014, **63**, 18–26.
24 T. Alerte, J. P. Edwards, C. M. Gabardo, C. P. O'Brien, A. Gaona, J. Wicks, A. Obradović, A. Sarkar, S. A. Jaffer, H. L. MacLean, D. Sinton and E. H. Sargent, *ACS Energy Lett.*, 2021, **6**, 4405–4412.
25 J. B. Greenblatt, D. J. Miller, J. W. Ager, F. A. Houle and I. D. Sharp, *Joule*, 2018, **2**, 381–420.
26 M. Ma, E. L. Clark, K. T. Therkildsen, S. Dalsgaard, I. Chorkendorff and B. Seger, *Energy Environ. Sci.*, 2020, **13**, 977–985.
27 Y. Xu, J. P. Edwards, S. Liu, R. K. Miao, J. E. Huang, C. M. Gabardo, C. P. O'Brien, J. Li, E. H. Sargent and D. Sinton, *ACS Energy Lett.*, 2021, **6**, 809–815.
28 J. Y. T. Kim, P. Zhu, F.-Y. Chen, Z.-Y. Wu, D. A. Cullen and H. Wang, *Nat. Catal.*, 2022, **5**, 288–299.
29 K. Yang, M. Li, S. Subramanian, M. A. Blommaert, W. A. Smith and T. Burdyny, *ACS Energy Lett.*, 2021, **6**, 4291–4298.
30 J. A. Rabinowitz and M. W. Kanan, *Nat. Commun.*, 2020, **11**, 5231.
31 L. Ge, H. Rabiee, M. Li, S. Subramanian, Y. Zheng, J. H. Lee, T. Burdyny and H. Wang, *Chem*, 2022, **8**, 663–692.
32 S. Garg, M. Li, T. Hussain, M. N. Idros, Y. Wu, X. S. Zhao, G. G. X. Wang and T. E. Rufford, *ACS Appl. Mater. Interfaces*, 2022, DOI: **10.1021/acsami.2c05918**.
33 I. Sullivan, A. Goryachev, I. A. Digdaya, X. Li, H. A. Atwater, D. A. Vermaas and C. Xiang, *Nat. Catal.*, 2021, **4**, 952–958.
34 R. Sharifian, R. M. Wagterveld, I. A. Digdaya, C. Xiang and D. A. Vermaas, *Energy Environ. Sci.*, 2021, **14**, 781–814.
35 O. Gutiérrez-Sánchez, B. Bohlen, N. Daems, M. Bulut, D. Pant and T. Breugelmans, *ChemElectroChem*, 2022, **9**, e202101540.
36 M. Li, E. Irtem, H. P. I. v. Montfort and T. Burdyny, *ChemRxiv*, 2021, DOI: **10.26434/chemrxiv-2021-33k4d**.
37 G. Lee, Y. C. Li, J.-Y. Kim, T. Peng, D.-H. Nam, A. S. Rasouli, F. Li, M. Luo, A. H. Ip, Y.-C. Joo and E. H. Sargent, *Nat. Energy*, 2021, **6**, 46–53.
38 H. Yamada, *Polym. J.*, 2021, **53**, 93–102.
39 G. T. Rochelle, *Science*, 2009, **325**, 1652–1654.
40 B. Dutcher, M. Fan and A. G. Russell, *ACS Appl. Mater. Interfaces*, 2015, **7**, 2137–2148.
41 1930.
42 D. M. D'Alessandro, B. Smit and J. R. Long, *Angew. Chem., Int. Ed.*, 2010, **49**, 6058–6082.
43 P. W. J. Derks, P. J. G. Huttenhuis, C. van Aken, J.-H. Marsman and G. F. Versteeg, *Energy Procedia*, 2011, **4**, 599–605.
44 J. P. Jakobsen, J. Krane and H. F. Svendsen, *Ind. Eng. Chem. Res.*, 2005, **44**, 9894–9903.
45 L. A. Diaz, N. Gao, B. Adhikari, T. E. Lister, E. J. Dufek and A. D. Wilson, *Green Chem.*, 2018, **20**, 620–626.
46 M. C. Simoes, K. J. Hughes, D. B. Ingham, L. Ma and M. Pourkashanian, *Ind. Eng. Chem. Res.*, 2018, **57**, 2346–2352.
47 Z. Liang, K. Fu, R. Idem and P. Tontiwachwuthikul, *Chin. J. Chem. Eng.*, 2016, **24**, 278–288.
48 E. Gjernes, S. Pedersen, T. Cents, G. Watson, B. F. Fostås, M. I. Shah, G. Lombardo, C. Desvignes, N. E. Flø, A. K. Morken, T. de Cazenove, L. Faramarzi and E. S. Hamborg, *Energy Procedia*, 2017, **114**, 1146–1157.
49 U. E. Aronu, S. Gondal, E. T. Hessen, T. Haug-Warberg, A. Hartono, K. A. Hoff and H. F. Svendsen, *Chem. Eng. Sci.*, 2011, **66**, 6393–6406.
50 I. Kim, K. A. Hoff and T. Mejdell, *Energy Procedia*, 2014, **63**, 1446–1455.
51 K. G. Joback, J. R. Heberle and A. S. Bhown, *Energy Procedia*, 2017, **114**, 1689–1708.

52 C.-T. Dinh, T. Burdyny, M. G. Kibria, A. Seifitokaldani, C. M. Gabardo, F. P. G. d. Arquer, A. Kiani, J. P. Edwards, P. D. Luna, O. S. Bushuyev, C. Zou, R. Quintero-Bermudez, Y. Pang, D. Sinton and E. H. Sargent, *Science*, 2018, **360**, 783–787.
53 K. Yang, R. Kas and W. A. Smith, *J. Am. Chem. Soc.*, 2019, **141**, 15891–15900.
54 N. S. Matin, J. E. Remias, J. K. Neathery and K. Liu, *Ind. Eng. Chem. Res.*, 2012, **51**, 6613–6618.
55 B. Lv, B. Guo, Z. Zhou and G. Jing, *Environ. Sci. Technol.*, 2015, **49**, 10728–10735.
56 M. Du, *AIP Conf. Proc.*, 2017, **1864**, 020091.
57 A. J. Welch, E. Dunn, J. S. DuChene and H. A. Atwater, *ACS Energy Lett.*, 2020, **5**, 940–945.
58 M. Dunwell, Q. Lu, J. M. Heyes, J. Rosen, J. G. Chen, Y. Yan, F. Jiao and B. Xu, *J. Am. Chem. Soc.*, 2017, **139**, 3774–3783.
59 W. Deng, T. Yuan, S. Chen, H. Li, C. Hu, H. Dong, B. Wu, T. Wang, J. Li, G. A. Ozin and J. Gong, *Fundam. Res.*, 2021, **1**, 432–438.
60 L. Chen, F. Li, Y. Zhang, C. L. Bentley, M. Horne, A. M. Bond and J. Zhang, *ChemSusChem*, 2017, **10**, 4109–4118.
61 E. Pérez-Gallent, C. Vankani, C. Sánchez-Martínez, A. Anastasopol and E. Goetheer, *Ind. Eng. Chem. Res.*, 2021, **60**, 4269–4278.
62 N. Ahmad, Y. Chen, X. Wang, P. Sun, Y. Bao and X. Xu, *Renewable Energy*, 2022, **189**, 444–453.
63 Z. Zhang, E. W. Lees, S. Ren, A. Huang and C. P. Berlingette, *ChemRxiv*, 2021, DOI: **10.26434/chemrxiv.13665074.v1**.
64 C. P. O'Brien, R. K. Miao, S. Liu, Y. Xu, G. Lee, A. Robb, J. E. Huang, K. Xie, K. Bertens, C. M. Gabardo, J. P. Edwards, C.-T. Dinh, E. H. Sargent and D. Sinton, *ACS Energy Lett.*, 2021, **6**, 2952–2959.
65 T. Li, E. W. Lees, M. Goldman, D. A. Salvatore, D. M. Weekes and C. P. Berlinguette, *Joule*, 2019, **3**, 1487–1497.
66 T. Li, E. W. Lees, Z. Zhang and C. P. Berlinguette, *ACS Energy Lett.*, 2020, **5**, 2624–2630.
67 E. W. Lees, J. C. Bui, D. Song, A. Z. Weber and C. P. Berlinguette, *ACS Energy Lett.*, 2022, **7**, 834–842.
68 R. Kas, K. Yang, G. P. Yewale, A. Crow, T. Burdyny and W. A. Smith, *Ind. Eng. Chem. Res.*, 2022, **61**, 10461–10473.
69 A. Khurram, L. Yan, Y. Yin, L. Zhao and B. M. Gallant, *J. Phys. Chem. C*, 2019, **123**, 18222–18231.
70 M. Li, S. Garg, X. Chang, L. Ge, L. Li, M. Konarova, T. E. Rufford, V. Rudolph and G. Wang, *Small Methods*, 2020, **4**, 2000033.
71 M. Abdinejad, Z. Mirza, X.-a. Zhang and H.-B. Kraatz, *ACS Sustainable Chem. Eng.*, 2020, **8**, 1715–1720.
72 L. Li, J. Yang, L. Li, Y. Huang and J. Zhao, *Electrochim. Acta*, 2022, **402**, 139523.
73 N. Ahmad, X. Wang, P. Sun, Y. Chen, F. Rehman, J. Xu and X. Xu, *Renewable Energy*, 2021, **177**, 23–33.
74 M. N. Hossain, S. Ahmad, I. S. da Silva and H.-B. Kraatz, *Chem. – Eur. J.*, 2021, **27**, 1346–1355.
75 J. H. Kim, H. Jang, W. Choi, H. Yun, E. C. Lee, D. Kim, J. W. Kim, S. Y. Lee and Y. J. Hwang, *Res. Sq.*, 2022, DOI: **10.21203/rs.3.rs-1310811/v1**.
76 S.-J. Han and J.-H. Wee, *J. Chem. Eng. Data*, 2016, **61**, 712–720.
77 R. J. Gilliam, J. W. Graydon, D. W. Kirk and S. J. Thorpe, *Int. J. Hydrogen Energy*, 2007, **32**, 359–364.
78 E. W. Lees, M. Goldman, A. G. Fink, D. J. Dvorak, D. A. Salvatore, Z. Zhang, N. W. X. Loo and C. P. Berlinguette, *ACS Energy Lett.*, 2020, **5**, 2165–2173.
79 Z. Zhang, E. W. Lees, F. Habibzadeh, D. A. Salvatore, S. Ren, G. L. Simpson, D. G. Wheeler, A. Liu and C. P. Berlinguette, *Energy Environ. Sci.*, 2022, **15**, 705–713.
80 M. Li, M. N. Idros, Y. Wu, T. Burdyny, S. Garg, X. S. Zhao, G. Wang and T. E. Rufford, *J. Mater. Chem. A*, 2021, **9**, 19369–19409.
81 H. Rabiee, L. Ge, X. Zhang, S. Hu, M. Li and Z. Yuan, *Energy Environ. Sci.*, 2021, **14**, 1959–2008.
82 Y. Wu, S. Garg, M. Li, M. N. Idros, Z. Li, R. Lin, J. Chen, G. Wang and T. E. Rufford, *J. Power Sources*, 2022, **522**, 230998.
83 R. N. Wenzel, *Ind. Eng. Chem.*, 1936, **28**, 988–994.
84 K. Yang, R. Kas, W. A. Smith and T. Burdyny, *ACS Energy Lett.*, 2021, **6**, 33–40.
85 Z. Xing, L. Hu, D. S. Ripatti, X. Hu and X. Feng, *Nat. Commun.*, 2021, **12**, 136.
86 A. G. Fink, E. W. Lees, Z. Zhang, S. Ren, R. S. Delima and C. P. Berlinguette, *ChemElectroChem*, 2021, **8**, 2094–2100.
87 M. M. Waegele, C. M. Gunathunge, J. Li and X. Li, *J. Chem. Phys.*, 2019, **151**, 160902.
88 M. C. O. Monteiro, F. Dattila, B. Hagedoorn, R. García-Muelas, N. López and M. T. M. Koper, *Nat. Catal.*, 2021, **4**, 654–662.
89 S. Ringe, E. L. Clark, J. Resasco, A. Walton, B. Seger, A. T. Bell and K. Chan, *Energy Environ. Sci.*, 2019, **12**, 3001–3014.
90 L. D. Chen, M. Urushihara, K. Chan and J. K. Nørskov, *ACS Catal.*, 2016, **6**, 7133–7139.
91 J. Resasco, L. D. Chen, E. Clark, C. Tsai, C. Hahn, T. F. Jaramillo, K. Chan and A. T. Bell, *J. Am. Chem. Soc.*, 2017, **139**, 11277–11287.
92 M. C. O. Monteiro, M. F. Philips, K. J. P. Schouten and M. T. M. Koper, *Nat. Commun.*, 2021, **12**, 4943.
93 D. Kim, W. Choi, H. W. Lee, S. Y. Lee, Y. Choi, D. K. Lee, W. Kim, J. Na, U. Lee, Y. J. Hwang and D. H. Won, *ACS Energy Lett.*, 2021, **6**, 3488–3495.
94 S.-F. Zhao, M. Horne, A. M. Bond and J. Zhang, *J. Phys. Chem. C*, 2016, **120**, 23989–24001.

95 S. Garg, M. Li, T. E. Rufford, L. Ge, V. Rudolph, R. Knibbe, M. Konarova and G. G. X. Wang, *ChemSusChem*, 2020, **13**, 304–311.
96 S. Garg, M. Li, Y. Wu, M. N. Idros, H. Wang, A. J. Yago, L. Ge, G. G. X. Wang and T. E. Rufford, *ChemSusChem*, 2021, **14**, 2601–2611.
97 S. Banerjee, X. Han and V. S. Thoi, *ACS Catal.*, 2019, **9**, 5631–5637.
98 H. P. I. v. Montfort and T. Burdyny, *ACS Energy Lett.*, 2022, **7**, 2410–2419.
99 E. L. Clark, J. Resasco, A. Landers, J. Lin, L.-T. Chung, A. Walton, C. Hahn, T. F. Jaramillo and A. T. Bell, *ACS Catal.*, 2018, **8**, 6560–6570.
100 L.-C. Weng, A. T. Bell and A. Z. Weber, *Phys. Chem. Chem. Phys.*, 2018, **20**, 16973–16984.